IEEE Access
Multidisciplinary | Rapid Review | Open Access Journal

Received 14 September 2022, accepted 1 January 2023, date of publication 16 January 2023, date of current version 25 January 2023.

Digital Object Identifier 10.1109/ACCESS.2023.3237763

RESEARCH ARTICLE

Development of Dummy Based on Impedance Properties of Human Soft Tissue Using a Nonlinear Viscoelastic Model

JIAN LIU[1], YOJI YAMADA[1,2], (Member, IEEE), YASUHIRO AKIYAMA[3], (Member, IEEE), SHOGO OKAMOTO[4], (Member, IEEE), AND YUMENA IKI[5]

[1]Department of Mechanical Systems Engineering, Nagoya University, Nagoya 464-8603, Japan
[2]Toyota College, National Institute of Technology, Toyota 471-0067, Japan
[3]Faculty of Textile Science and Technology, Shinshu University, Ueda 386-8567, Japan
[4]Department of Computer Science, Tokyo Metropolitan University, Hino 191-0065, Japan
[5]Denso Corporation, Kariya 448-0029, Japan

Corresponding author: Jian Liu (liu.jian@k.mbox.nagoya-u.ac.jp)

This work was supported in part by the Ministry of Economy, Trade and Industry, Japan, under Grant SSU53-437-sen46, Project Name: "International Standardization of Safety Test Methods for Minor Hand Injuries Based on Actual Use Cases of Human-Collaborating Machines;" in part by the Aichi Science and Technology Foundation, Japan, Project Name: R7 of the "Knowledge Hub Aichi."

This work involved human subjects or animals in its research. Approval of all ethical and experimental procedures and protocols was granted by the Ethics Committee of the Department of Engineering of Nagoya University under Approval No. 18-14.

ABSTRACT Securing human safety in a physical human–robot interaction (pHRI) has been extensively studied to allow for the expansion of robotic applications. Dummies with the same impedance properties as those of human soft tissues are suitable substitutes for the validation of the safety assurance of the pHRI experiment. This study demonstrated the development process of dummies with high biofidelity. A psychophysiological experiment was designed to replicate the clamping scenario, and the center of the palm, thenar eminence, and forefinger pad were selected as three soft tissues of the human hand to be impacted to obtain the dynamic response of the contact force. A nonlinear five-element viscoelastic model was developed to quantify the viscoelasticity of the three soft tissues through curve fitting of the contact force. Subsequently, three dummies were fabricated using a polyurethane resin material. The biofidelity of the dummies was examined via a parametric comparison with the soft tissues and curve comparisons to examine whether the steady-state force and the dynamic response of the contact force were located within the corresponding ranges enclosed by the calibration curves of the soft tissues. All three dummies showed high biofidelity in the case where the steady-state force exceeded approximately 5 N, even though they have different nonlinearity of elasticity from that of soft tissues.

INDEX TERMS Physical human–robot interaction, impedance property, viscoelasticity, dummy development, nonlinear viscoelastic model, human soft tissue.

I. INTRODUCTION

As robots are being applied in various fields, removal of the barriers between humans and robots is being increasingly investigated [1]. Thus, humans and robots would share a physical environment, thereby inevitably increasing the possibility of the physical human–robot interaction (pHRI) [2], [3]. Ensuring human safety in a human–robot coexistence environment is currently one of the most important fields in robotics [4]. Certain studies regarding safe pHRIs were based on validation experiments conducted directly on human body parts [5], [6], [7]. To a certain degree, the experiments on human subjects sufficiently validated the effectiveness of the pHRI framework; however, their safety must be guaranteed,

The associate editor coordinating the review of this manuscript and approving it for publication was Jingang Jiang.

and an injury validation experiment (e.g., slight injury) is prohibited and unattainable.

In recent years, the injury criteria for different human body parts in pHRI have been stressed in the ISO documentation [8], [9]. Owing to ethical prohibition, injury criteria were estimated through substitutes of the human soft tissue, such as porcine skin [10], [11], [12]. Dummy skins have been considered as suitable substitutes for human soft tissue and used in injury validation experiments. The transferability of a Hybrid III dummy from the automotive industry for use in robotics was demonstrated by Oberer and Schraft [13]. Haddadin et al. [14], [15] investigated the influence of robot mass and velocity on the injury indices using a Hybrid III dummy and developed a head–neck dummy consisting of a compliant covering and spring. These studies mainly focused on the head injury criterion, and the dummy had low biofidelity owing to a higher stiffness of the head–neck structure than that of humans [16].

Therefore, for the validation of safety assurance of the pHRI experiment, dummies that represent the same mechanical properties as those of the human soft tissue are primarily imperative as suitable substitutes. This also indicates the possibility for large quantity production, convenience for experiments, and high biofidelity, thereby guaranteeing efficiency. In a more advanced version, pressure/stress distribution sensors can be inserted to measure the pressure of different soft tissue layers for further study [17], [18].

The biofidelity of dummies should be embodied in the viscoelasticity because the human soft tissue intrinsically possesses creep, stress relaxation, and hysteresis behaviors [19]. Viscoelasticity is crucial for quantifying the severity of injury caused by pHRI, such as the allowable transient force and power [9], [20] and the total transferred energy [11], [12].

To model the viscoelasticity of soft tissue, precise viscoelastic finite element models were proposed in previous studies [21], [22], [23]. Nevertheless, the application of these models to dummy development is difficult, thereby necessitating a simplified mechanical model that has a brief representation of elasticity and viscosity and is suitable for material production. An alternative would be such models to be combinations of the Maxwell and Voigt bodies, which have been applied in many research studies [24], [25], [26], [27]. However, in the aforementioned studies, the method for measuring the viscoelastic properties of soft tissue was based on the force–displacement (or stress–strain) relation, in other words, an admittance property from the viewpoint of pHRI modeling [28]. The impedance and admittance properties describe the input–output properties of a dynamic system and are inverse to each other, but the inverse operation is difficult to carry out if the system possesses nonlinearity. Most industrial robots are operated under motion control. When the human soft tissue is clamped by an industrial robot, the contact force is generated by the compressive displacement. Regarding the soft tissue as a dynamic system, the compressive displacement and response contact force are the input and output, respectively. The impedance property is exhibited in most cases of the pHRI. Therefore, the impedance property of human soft tissue is more applicable in dummy development. Aso et al. [29] measured the impedance properties of the human thigh in the frequency domain, but no specific viscoelastic model was proposed. A linear four-element viscoelastic model was used by Nakazawa et al. [30] to describe the impedance property of the human fingertip.

Our previous study [31] proposed a nonlinear two-layer viscoelastic model for analyzing the mechanical property of the human soft tissue. However, the derivation of an analytic expression for the model was difficult, and the redundancy of optimal solutions for curve fitting was disregarded. These noticeable points are addressed in this study by proposing a nonlinear five-element viscoelastic model.

This paper proposes a development process of high-biofidelity dummies as substitutes for the human soft tissue for hazardous pHRI experiments. The rest of the paper is organized as follows: First, the human hand was selected as the object of study, given that it is one of the body parts that are most likely to be impacted in a human–robot collaboration operation. A psychophysiological experiment was conducted to measure the dynamic response of the contact force of human hands under the worst case of pHRI: the clamping scenario. Second, a nonlinear viscoelastic model was developed to quantify the viscoelasticity of the soft tissues of the human hand based on five viscoelastic parameters. Third, based on the analysis results, dummies were fabricated using a polyurethane resin material. Finally, the biofidelity of the dummies was examined via the following two approaches: a comparison between the viscoelastic parameters of the dummies and those of the soft tissues, and curve comparisons to determine whether the steady-state force and the dynamic response of the contact force of the dummies are located within the corresponding ranges enclosed by the calibration curves of the soft tissues.

II. PSYCHOPHYSIOLOGICAL EXPERIMENT

The clamping scenario is the worst case of the pHRI, and the dynamic response of the contact force generated in the dynamic impact is stressed in ISO 15066 [9] as a factor affecting human safety. Therefore, the psychophysiological experiment designed in this study aimed to establish a methodology for replicating a dynamic clamping scenario, where the human hand was clamped by a fixed obstacle and an approaching end effector of a robot [32]. The dynamic response of the contact force obtained through the impact experiment was analyzed using the proposed nonlinear viscoelastic model, and the viscoelasticity of the human hand was quantified using five viscoelastic parameters. The analysis results were used for the dummy development.

The associated safety standard [9] proposed several regions of the hand for validation. However, considering that clamping the dorsal side of the hand is hazardous, the palmar side was considered, and the center of the palm, forefinger pad,

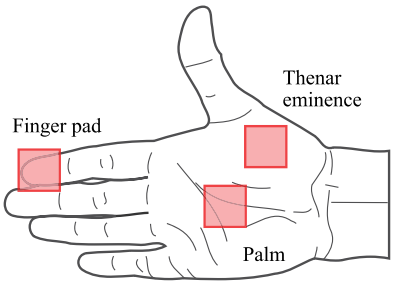

FIGURE 1. Three contact areas of the human hand, i.e., the center of a palm, thenar eminence, and forefinger pad, which are marked by red squares coinciding with the square contact surface of the impactor.

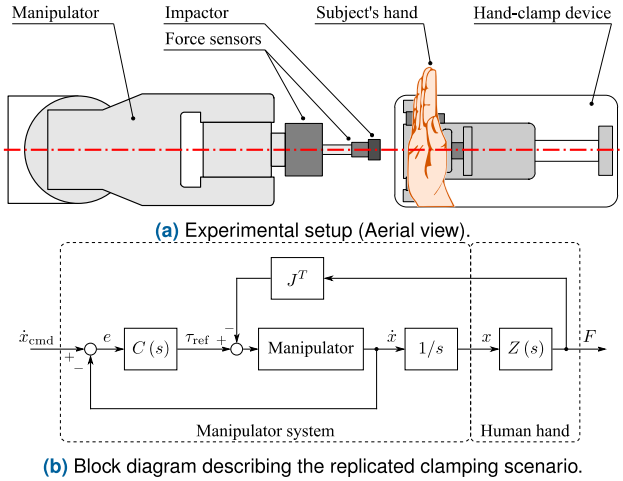

FIGURE 2. (a) Aerial view of the experimental setup for replicating the clamping scenario. The red dash-dotted line represents the centrosymmetric line of the hand-clamp device, which is also the impact direction. The hand-clamp device is shown in Fig. 3. (b) The block diagram describes the dynamic system, including the impactor and human hand in the replicated clamping scenario in (c).

and thenar eminence were chosen as specific areas in the impact experiment, as shown in Fig. 1.

The Ethics Committee of the Department of Engineering at Nagoya University (approval No. 18-14) approved this psychophysiological experimental method.

A. EXPERIMENT APPARATUS

A manipulator (VS-050, DENSO WAVE Incorporated, Japan) was used to provide precise compressive displacement and contact velocity. A six-axis force sensor (LFS100-500-10-U, Nippon Liniax Co. Ltd., Japan) attached on the end effector was used to measure the contact force. A square impactor with a size of 14 × 14 mm^2 was attached on the six-axis force. The impact orientation was organized along the centrosymmetric line of the developed device to allow for the application of normal forces, as shown in Fig. 2. The six-axis force sensor can measure the contact force and wrench in Cartesian coordinates; therefore, by checking the contact force in the three axes, the normal direction of the contact force was confirmed.

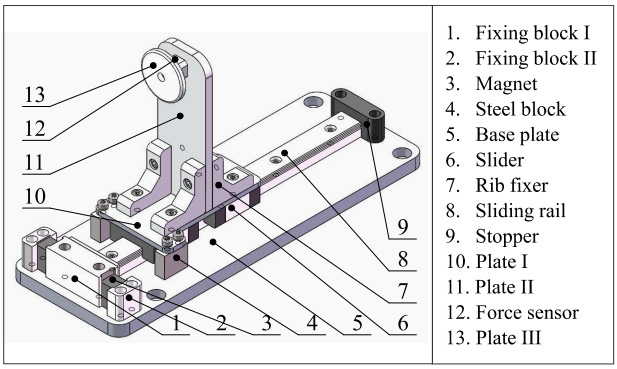

FIGURE 3. Structure of the device that mechanically secures the safety of human hands.

As shown in Fig. 3, a device to mechanically secure the safety of human hands in the impact experiment was developed. Under normal working conditions, two magnets (component 3) cling to the steel block (component 4) to achieve an attractive force of 100 N, and thus, the removable body (components 4 and 10–13) is kept close to component 1. The plate (component 13) supports the hand, as shown in Fig. 2. If the impact applied to the hand is sufficiently intense to cause the contact force to exceed the threshold value of 100 N, the removable body breaks away from the magnets and slides to component 9. Therefore, this device helps the human hand to slide away from the collision to limit the maximum amount of contact force within 100 N.

As an additional safety measure, software monitored the contact force applied via two force sensors (9313AA1, The Kistler Group, Japan) mounted on the impactor and developed device.

B. EXPERIMENT DESIGN

The procedure of the experiment is as follows:

(a) The dorsal side of the hand is maintained in contact with the circular plate (component 13 in Fig. 3) of the device, as shown in Fig. 2, and the hand is kept relaxed to avoid the potential influences of muscle activations.
(b) The impactor is gradually moved to clamp the specific contact area, and the compressive displacement is adjusted to meet the desired steady-state force.
(c) The impactor is moved a specified distance from the specific contact area, e.g., 300 mm.
(d) The impactor is moved with the desired contact velocity to impact the specific contact area, then stopped for 10 s at the compressive displacement determined in step (b).
(e) Step (c) is repeated.

The steady-state force mentioned in step (b) indicates the steady-state phase of the contact force corresponding to the stress relaxation behavior of human soft tissue, as determined by the contact force after the impactor is stopped for 10 s. Additionally, after observing the contact force profile shown in Fig. 5, the 10 s period was chosen.

Human subjects determined the maximum steady-state force by marking their thresholds for discomfort or unbearable pain due to repeated impact. As a result, the steady-state force was set at 5, 10, and 15 N. Because the human subjects felt pain as the steady-state force reached 20 N, the maximum steady-state force was set at 15 N, which is below 20 N. The contact velocities were set at 10 and 250 mm/s for quasi-static and dynamic contacts, respectively [33].

As mentioned above, the manipulator was employed to realize precise compressive displacement and contact velocity. The entire dynamic system, including the manipulator and a human hand, is explained using a block diagram, as shown in Fig. 2(b). The controller, $C(s)$, generates a reference torque, τ_{ref}, to move the end effector and resist the reaction torque, $J^T F$, where J and F denote the Jacobean matrix and contact force, respectively. The difference between the command velocity, $\dot{x}_{\mathrm{cmd}}$, and response velocity, $\dot{x}$, that is, the error, e, is reduced to approximately zero. The end effector impacts the human hand under a compressive displacement, x, and receives a response contact force, F, owing to the impedance, $Z(s)$, of the human hand. This motion controller is a closed-loop system provided by DENSO WAVE Incorporated, and the precision reaches ± 0.02 mm in the operational-space motion tracking. In this study, the dummy development necessitates the analysis of the impedance of the soft tissues on the human hand, which is regarded as the property of a dynamic system where the compressive displacement, x, is the input and the contact force, F, the output.

Five healthy male human subjects participated in the experiments. Each contact condition involved three trials.

C. EXPERIMENT RESULTS

The profile of the contact force variation is shown in Fig. 4(b). A fast Fourier transform (FFT) was conducted to analyze the noise in the contact force signal, and the result is shown in Fig. 4(a). The noise appeared when the frequency was larger than 35 Hz. The comparison in Fig. 4(b) indicates that if the cutoff frequency was lower than 35 Hz, the waveform of the contact force signal was destroyed such that the sharp peak of the contact force was reduced and shifted. Therefore, the contact force data was denoised using a second-order digital filter with a cut-off frequency of 35 Hz. The filtered contact forces of one subject's palm are shown in Fig. 5.

Figure 5 shows that the tendencies of force variation were similar despite differences among the steady-state forces. Specifically, a peak value of the contact force occurred when the impactor reached the predetermined compressive displacement. The contact force then gradually decreased to a constant value (the steady-state force). It can be inferred that the steady-state force is influenced by the stiffness or elasticity of the soft tissue, while the peak value of the response force with its decline shows the viscosity.

III. NONLINEAR VISCOELASTIC MODEL

The dynamic response of the contact force of the three soft tissues was obtained through the psychophysiological

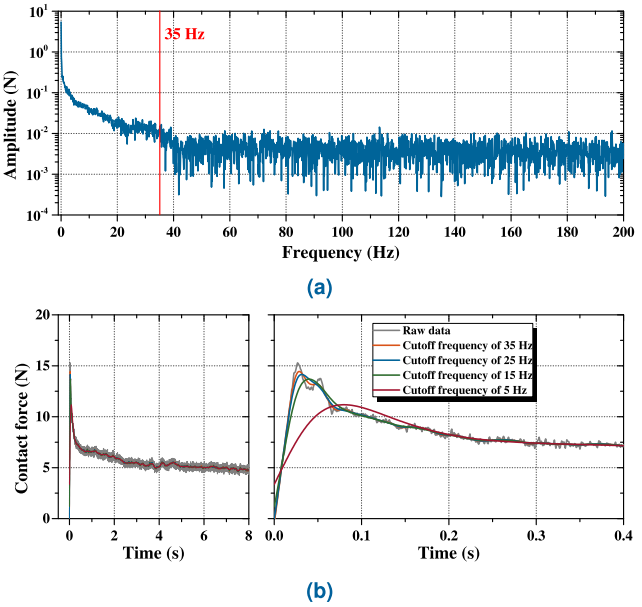

FIGURE 4. (a) FFT result of the contact force signal. The red line denotes the frequency of 35 Hz. (b) Comparison among the raw data and filtered contact force with a cutoff frequency of 35, 25, 15, and 5 Hz. The right graph shows details around the peak value timing of the left graph.

experiments. A nonlinear viscoelastic model was developed to quantitatively analyze the viscoelasticity of the soft tissues as well as the developed dummies. By using the model, calibration curves of both the steady-state force and dynamic response of the contact force were provided to examine the biofidelity of the dummies.

A. CONVENTIONAL LINEAR VISCOELASTIC MODEL

The five-element Maxwell model is composed of two Maxwell bodies and one Hookean spring connected in parallel, as shown in Fig. 6, with the definition of the elastic parameters k_1, k_2, and k_3, and viscous parameters c_2 and c_3. The mathematical expressions of the five-element model are as follows:

$$x(t) = \begin{cases} vt & 0 \le t < t_{\mathrm{p}} \\ vt_{\mathrm{p}} & t_{\mathrm{p}} \le t \end{cases}, \tag{1}$$

$$F(t) = \begin{cases} k_1 vt + \sum_{i=2}^{3} c_i v\left[1 - \exp\left(-\frac{k_i}{c_i} t\right)\right] & 0 \le t < t_{\mathrm{p}} \\ k_1 vt_{\mathrm{p}} + \sum_{i=2}^{3} \left\{ c_i v\left[1 - \exp\left(-\frac{k_i}{c_i} t_{\mathrm{p}}\right)\right] \times \exp\left(-\frac{k_i}{c_i}\left(t - t_{\mathrm{p}}\right)\right) \right\} & t_{\mathrm{p}} \le t \end{cases}, \tag{2}$$

$$F_{\mathrm{s}} = k_1 x\left(t_{\mathrm{p}}\right), \tag{3}$$

where x denotes the compressive displacement, v the contact velocity, F the contact force, F_{s} the steady-state contact force, and t_{p} the peak value timing (or stop timing).

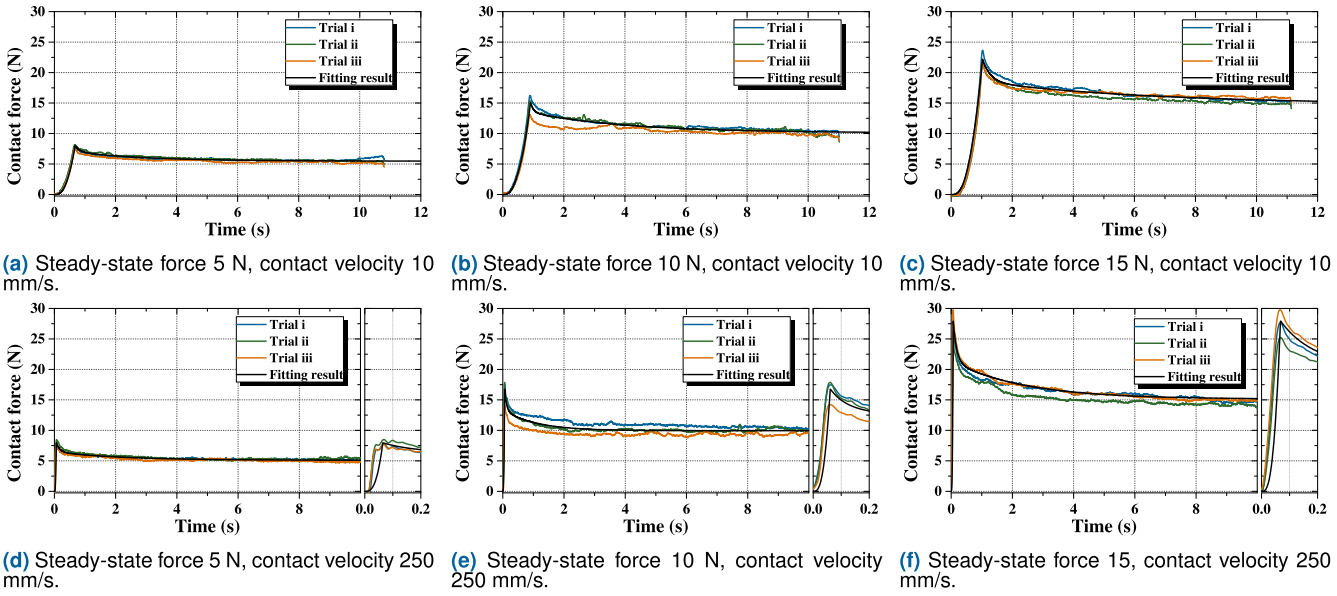

(a) Steady-state force 5 N, contact velocity 10 mm/s. (b) Steady-state force 10 N, contact velocity 10 mm/s. (c) Steady-state force 15 N, contact velocity 10 mm/s.

(d) Steady-state force 5 N, contact velocity 250 mm/s. (e) Steady-state force 10 N, contact velocity 250 mm/s. (f) Steady-state force 15, contact velocity 250 mm/s.

FIGURE 5. Profiles of the contact force variation of one subject's palm and fitting results by using the nonlinear model in equation (5). The contact condition of figures from (a) to (f) is: steady-state force of 5, 10, 15, 5, 10, and 15 N, and contact velocity of 10, 10, 10, 250, 250, and 250 mm/s, respectively. In (d)–(f), the graph on the right side shows the rising phase.

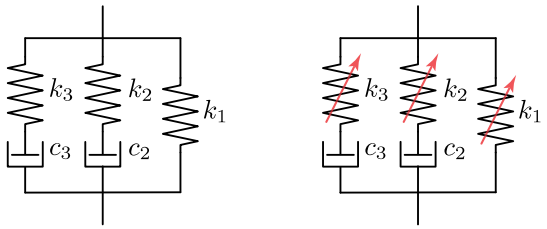

(a) Linear model. (b) Nonlinear model.

FIGURE 6. Linear and nonlinear five-element generalized Maxwell models. In (a) and (b), parameters k_1, k_2, and k_3 are defined as the stiffness of the three springs, and parameters c_2 and c_3 are the damping ratios of the two dampers. In (b), the red arrows indicate that the stiffness of the three springs is nonlinear.

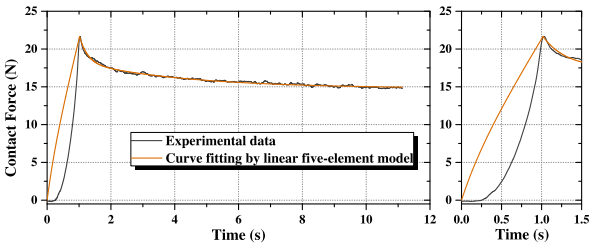

FIGURE 7. Comparison between the experimental data and curve fitting result of the linear five-element model. The graph on the right side shows details of the rising phase of the contact force.

Equation (2) shows that the variation in the response force is divided into two parts based on the peak value timing t_p, which coincides with the rising and attenuation phases of the contact force in Fig. 5. However, the rising phase of the curve of best fit by the linear model was convex and differed from that of the experimental results, as shown in Fig. 7. This linear model fails to express the mechanical properties of human soft tissue; however, it was first considered for fitting the attenuation phase.

B. PROPOSED NONLINEAR VISCOELASTIC MODEL

Even though the attenuation phase was perfectly matched, a set of generalized parameters that equally describe the contact force in arbitrary contact conditions was intended to be revealed. The relationships among five viscoelastic parameters and contact conditions from one subject's palm are summarized statistically in Fig. 8 as an example.

In Fig. 8(a), three elastic parameters were observed to have an increasing trend with respect to the compressive displacement. In this case, a square polynomial can perfectly describe the relation for generalizing elastic parameters as follows:

$$k_i = \gamma_i x^2 \quad (i = 1, 2, 3), \tag{4}$$

where γ_i is a constant coefficient for k_i. The fitting curve for each elastic parameter k_i was obtained by using Equation (4) and is shown in Fig. 8(a) for comparison.

Because the elastic parameter k_1 only contributes to the steady-state force corresponding to Equation (3), it is only relative to the compressive displacement. The relationship between k_1 and the contact velocity was not considered. Further descriptions worthy of special mention cannot be made for Figs. 8(b)–(e). Although a downward trend with respect to the contact velocity was observed in Figs. 8(f) and 8(g), generalizing the relationship between the viscous parameters and contact velocity necessitates additional contact velocity settings and was not considered.

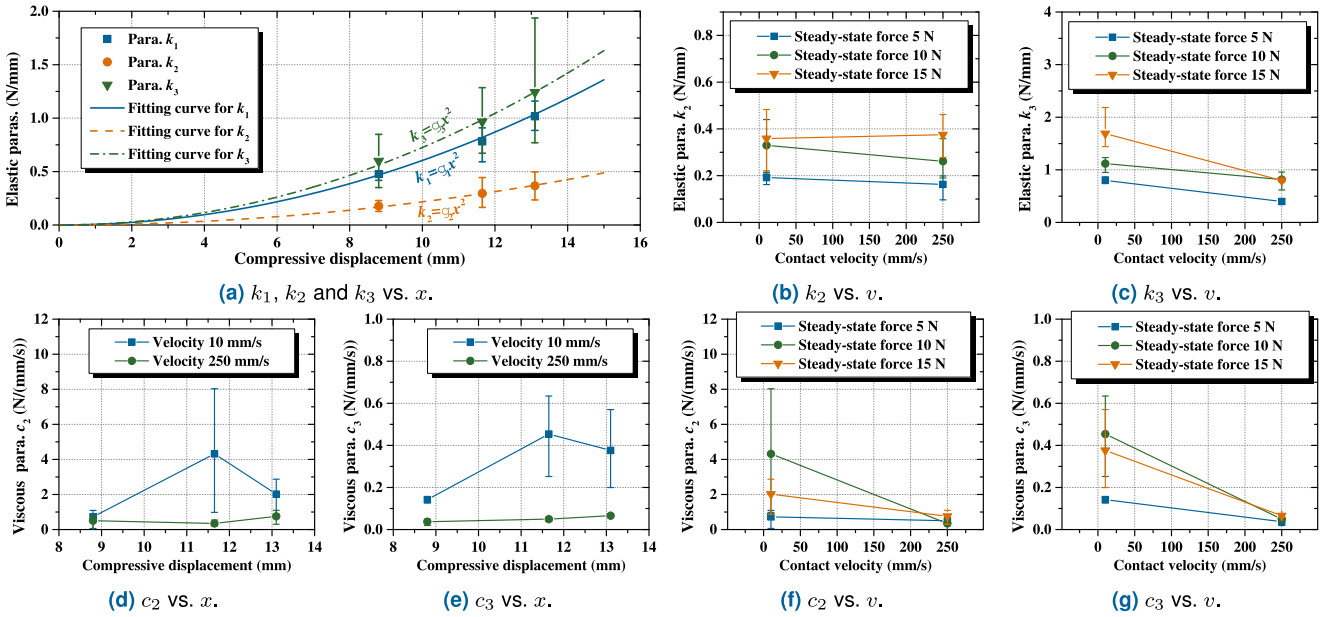

FIGURE 8. Relationships between contact conditions and parameters k_1, k_2, k_3, c_2, and c_3.

Considering the nonlinearity of the elastic parameters, a nonlinear five-element generalized Maxwell model was obtained and is shown in Fig. 6(b). By inserting Equation (4), Equations (2) and (6) are rewritten as follows:

$$F(t)=\begin{cases}\gamma_1(vt)^3+\sum_{i=2}^{3}c_iv\left[1-\exp\left(-\frac{\gamma_i}{c_i}v^2t^3\right)\right] & 0\le t<t_{\mathrm{p}}\\ \gamma_1(vt_{\mathrm{p}})^3+\sum_{i=2}^{3}\left\{c_iv\left[1-\exp\left(-\frac{\gamma_i}{c_i}v^2t_{\mathrm{p}}^3\right)\right]\times \exp\left(-\frac{\gamma_i}{c_i}v^2t^2\left(t-t_{\mathrm{p}}\right)\right)\right\} & t_{\mathrm{p}}\le t\end{cases}, \tag{5}$$

$$F_{\mathrm{s}}=\gamma_1x^3\left(t_{\mathrm{p}}\right). \tag{6}$$

Using the nonlinear five-element generalized Maxwell model along with the trust region algorithm, the dynamic response of the contact force was fitted and is presented in Fig. 5. Consequently, according to the curve fitting results, the optimized parameters (γ_1, γ_2, γ_3, c_2, and c_3) of the three soft tissues are depicted in Fig. 9, and for comparison, those of the three dummies are shown as well.

IV. DUMMY DEVELOPMENT

Based on the quantitative analysis of the impedance properties of the three soft tissues, three dummies were fabricated using a polyurethane resin material. TANAC Co., Ltd. provided manufacturing technology support. The polyurethane resin was fabricated by two agents being mixed together and hardening. The principal agent and hardening agent consisted of a polyol and isocyanate, respectively. The two agents were poured into a silicone rubber mold, and the bubbles generated when stirring were eliminated by using a vacuum environment. The mixed agents were then hardened in a drying furnace. The chemical reaction formula is shown in Fig. 10.

The viscoelasticity of the polyurethane resin material was determined only by changing the weight ratio of the principal agent to the hardening agent: the larger the weight ratio, the higher is the stiffness of the polyurethane resin. Based on the steady-state elasticity of the soft tissues analyzed in Section III, a weight ratio of 100:15 was selected for the development of the three dummies, with a Young's modulus of 25 kPa. Dummies I, II, and III corresponded to the palm, thenar eminence, and forefinger pad, with thicknesses of 15, 20, and 5 mm, respectively. The length and width of each dummy were 150 and 120 mm, respectively. Dummy I is depicted in Fig. 10(b).

The viscoelasticities of the dummies were investigated via two approaches. The first approach entailed a comparison between the viscoelastic parameters of the dummies and those of the soft tissues, as described in Section IV-A. The nonlinear model indicates that the mechanical property of human soft tissues has a steady-state elasticity attributed to the parameter γ_1 and additional attenuated forces from the other four parameters. The second approach entailed curve comparisons to determine whether both the steady-state force and dynamic response of the contact force of the dummies are located at the corresponding ranges enclosed by the calibration curves of the soft tissues, as described in Sections IV-B and IV-C.

A. VISCOELASTIC PARAMETERS

Using the proposed nonlinear viscoelasticity model, the viscoelasticity values of the soft tissues and dummies were

quantified using the five parameters: γ_1, γ_2, γ_3, c_2, and c_3. The optimization results are shown in Fig. 9 for comparison.

As illustrated by Equation (6), only γ_1 is related to the steady-state elasticity. The magnitude of parameter γ_1 of dummy I was between the largest and smallest γ_1 values of the palms, and the same result was observed in dummy II. Dummies I and II show a steady-state elasticity representing the average elasticity of soft tissues. Parameter γ_1 of dummy III was larger than that of the forefinger pads; therefore, dummy III exhibits a large steady-state elasticity compared to the forefinger pads.

Parameters γ_2, γ_3, c_2, and c_3 are related to the additional attenuated force. Parameters γ_3 and c_3 of dummy II were larger than those of the thenar eminences. According to the nonlinear model, a large c_3 contributes to a large peak value in the rising phase, and a large γ_3 causes a smaller time constant of the attenuation phase. Consequently, a large peak value and a rapid attenuation tendency appear in the contact force. This coincides with the observation in Figs. 12(b) and 12(e). Furthermore, parameters γ_2 and c_2 of dummy III were smaller than those of the thenar eminences. A small peak value and a slow attenuation tendency appear, which is observed in Figs. 12(c) and 12(f). Dummies II and III exhibit a viscosity that differs from that of the soft tissues.

B. STEADY-STATE ELASTICITY

A dummy that mimics the mechanical properties of human soft tissue needs to first satisfy the steady-state elasticity. Due to individual differences, the values of γ_1 that were obtained from different human subjects vary within a range. The average values of parameter γ_1 shown in Fig. 9 were used to compute the steady-state force according to Equation (6). Figure 11 shows the calibration curves representing the variation of the steady-state force with respect to the compressive displacement. The light gray region enclosed by the leftmost and rightmost calibration curves denotes a range of the steady-state force, herein referred to as the steady-state force range.

To examine the biofidelity of the three dummies, the steady-state forces were measured using the same experimental apparatus shown in Fig. 2(a) and are depicted in Fig. 11 for comparison. As shown by the error bars in Fig. 11, the trial error for each of the three trials was small. The steady-state forces of dummies I, II, and III exceeded the curve of the largest γ_1 when the contact started. Owing to the material behavior, all three artificial dummies show higher elasticity than that of the three soft tissues in a contact case of small compressive displacements. As the compressive displacement increased, the steady-state forces of the three dummies entered the steady-state force range. All three dummies show low elasticity under a large compressive displacement.

The steady-state force of dummy III was located near the left edge of the steady-state force range when the compressive displacement was large, i.e., dummy III represents the case of the largest γ_1.

C. VISCOELASTICITY

The same impact experiments were conducted on the three dummies to show the performance of the contact force variation. For brevity, the experimental results with the contact condition of a steady-state force of 10 N are shown in Fig. 12. The contact force of human subjects was depicted in a highly generalized manner. According to Equation (5), the average values of parameters γ_1, γ_2, γ_3, c_2, and c_3 shown in Fig. 9 were regarded as a set of coefficients for computing the contact force. Figure 12 shows the calibration curves representing the variation of the contact force with respect to time. The light gray region enclosed by the uppermost and lowest calibration curves denotes a range of the contact force, herein referred to as the force variation range. The curve comparison for the dynamic response of the contact force is similar to that for the steady-state force.

At the beginning of the rising phase, the contact forces of the three dummies exceeded those of the human subjects; however, they entered into the force variation range at the end of the rising phase, as observed in Figs. 12(a)–(c). This is consistent with the observation that all three artificial dummies show a higher elasticity when the compressive displacement is small.

Dummies I and III exhibited a small peak in the contact force located in the force variation range, whereas dummy II exhibited a large peak that almost reached the upper edge of the force variation range. This indicates that dummy II has a higher viscosity when compared with that of dummies I and III.

V. DISCUSSIONS

A. PERFORMANCE OF THE NONLINEAR MODEL

Principles for selecting a viscoelastic model were discussed by Shellhammer et al. [34]. In particular, the viscoelastic model should have as few terms as possible without losing the performance of fitting viscoelastic behaviors, that is, the trade-off between the simplicity and accuracy of the model. To meet this requirement, the curve fitting was also tested on nonlinear three- and seven-element models. The three-element model has one Maxwell body, whereas the seven-element model has three Maxwell bodies. As shown in Fig. 13, the five- and seven-element models had the same fitting capacity both in the rising and attenuation phases, whereas the three-element model lost the fitting capacity in the attenuation phase. The five-element model exhibits advantages with respect to both simplicity and accuracy compared with seven- and three-element models, respectively.

For the rising phase of the contact force, introducing the nonlinearity of elastic parameters k_1, k_2, and k_3 changes the convexity of the rising phase to concavity, which was observed from the curve fitting results of the linear five-element model in Fig. 7 and the nonlinear five-element model in Fig. 13. Both the rising and attenuation phases were well matched in trials on different contact areas under different contact conditions, and the curve fitting results showed that

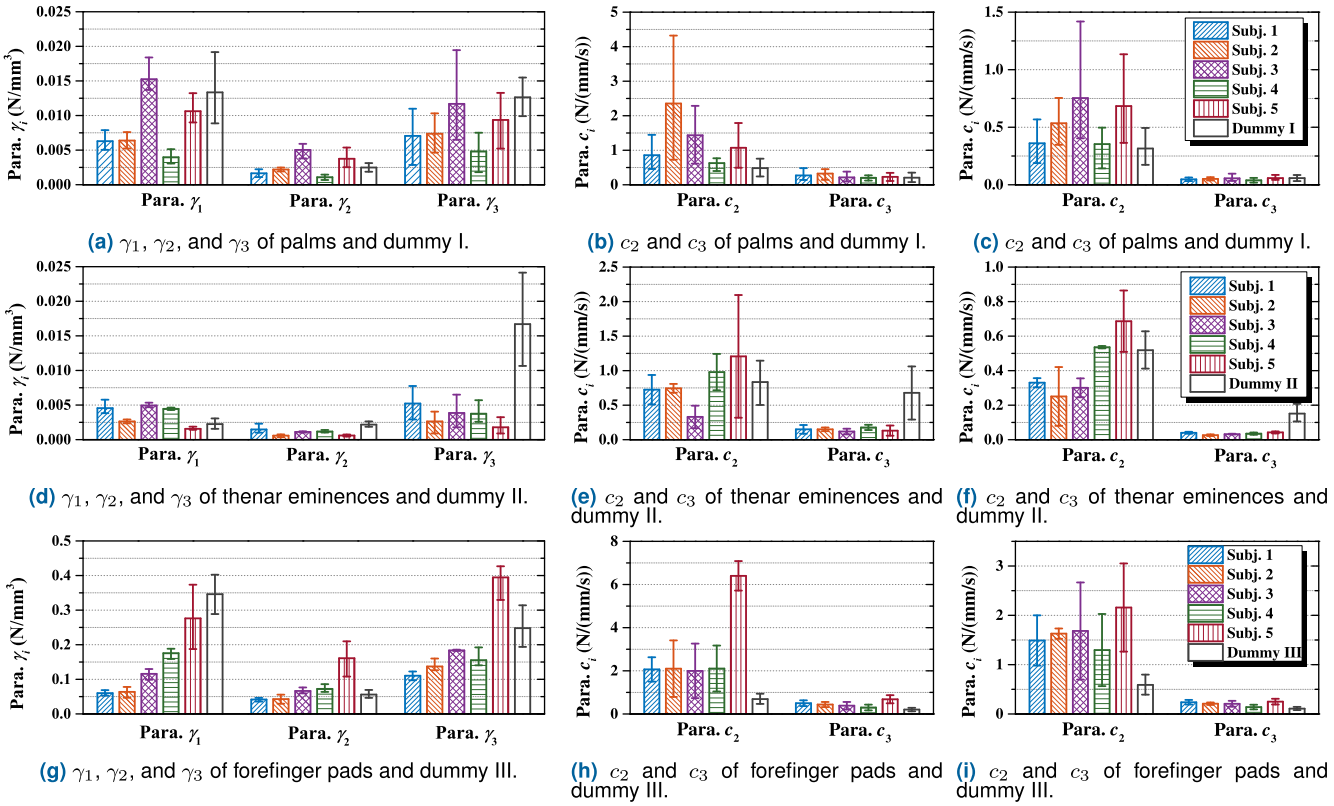

(a) γ_1, γ_2, and γ_3 of palms and dummy I. (b) c_2 and c_3 of palms and dummy I. (c) c_2 and c_3 of palms and dummy I.

(d) γ_1, γ_2, and γ_3 of thenar eminences and dummy II. (e) c_2 and c_3 of thenar eminences and dummy II. (f) c_2 and c_3 of thenar eminences and dummy II.

(g) γ_1, γ_2, and γ_3 of forefinger pads and dummy III. (h) c_2 and c_3 of forefinger pads and dummy III. (i) c_2 and c_3 of forefinger pads and dummy III.

FIGURE 9. Optimized parameters of palms and dummy I, thenar eminences and dummy II, and forefinger pads and dummy III. The optimization is conducted by curve fitting using the nonlinear five-element Maxwell model in Equation (5). Contact velocities of (b), (e), and (h) are 10 mm/s, while those of (c), (f), and (i) are 250 mm/s. The abbreviation "Subj. 1–5" is for "human subject 1–5" in the legend. For the legends of (a)-(c), see (c), (d)-(f), see (f), and (g)–(i), see (i).

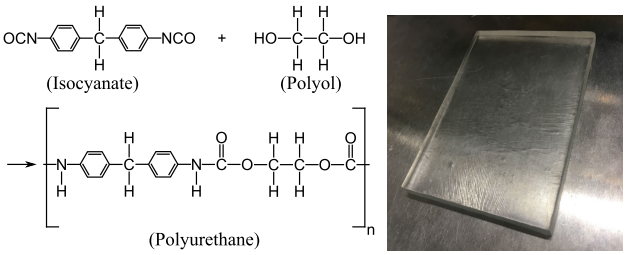

(a) (b)

FIGURE 10. (a) Chemical reaction formula of the principal agent (polyol), hardening agent (isocyanate), and polyurethane. (b) Photograph of dummy I with length, width, and thickness equal to 150, 120, and 15 mm, respectively.

the largest difference of approximately 2.3 N appeared at the peak contact force in the experiment.

Given that the parameter γ_1 is only related to the steady-state force F_s, it represents the elasticity of the human soft tissue. A large γ_1 value indicates high elasticity; for example, the palm of subject 4 is softer than that of subject 3, as observed in Fig. 9(a). Additionally, an interesting phenomenon was observed in Figs. 9(a), 9(d), and 9(g) with the magnitudes of the parameters γ_2 and γ_3 of the five subjects that had an identical variation tendency with that of the parameter γ_1. Specifically, the parameters γ_1, γ_2, and γ_3 may be inherently related, which may be interpreted as that in different subjects, the peak value $F\left(t_\mathrm{p}\right)$ of contact force correlates with the steady-state force F_s, and $F\left(t_\mathrm{p}\right) - F_\mathrm{s} < \left(\gamma_2 + \gamma_3\right) x^3\left(t_\mathrm{p}\right)$ based on equation (5).

The results indicate that parameter c_2 is always larger than c_3, while parameter γ_2 is always smaller than γ_3. Given that a small c_2 makes the damper release the contact force rapidly, a small c_2 and a large γ_2 provide a rapid attenuation of the contact force, which mainly contributes to the initial attenuation phase of the contact force, and vice versa.

Compared to the quasi-linear viscoelastic model proposed by Fung [19], our nonlinear model has advantages of physical significance, whereas the curve fitting performance for both models is similar. The quasi-linear viscoelastic model is formed as a convolution operating on a relaxation function and an instantaneous elastic response. It is a one-layer model and has no ordinary differential equation form. By contrast, the nonlinear model is easily understandable by the combination of nonlinear springs and dampers, such as in Fig. 6(b). Corresponding to the equivalent impedance method, the proposed model can be transformed into multi-layer models, such as a two-layer model [31]. The multi-layer model serves the development of multi-layer dummies, which results in the possibility of a high nonlinearity that cannot be realized

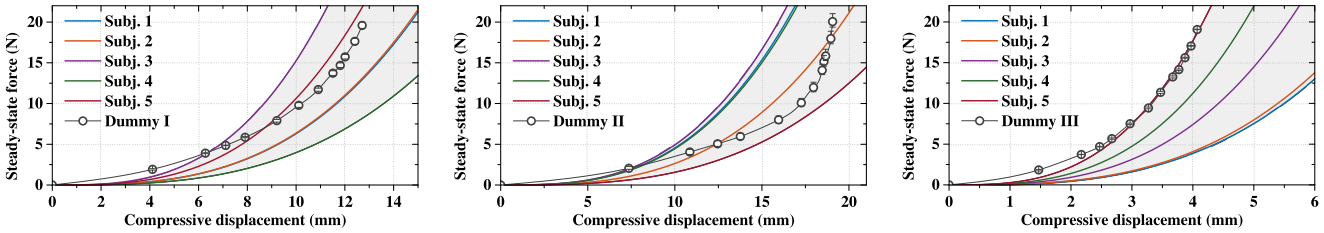

(a) Dummy I and palms. (b) Dummy II and thenar eminences. (c) Dummy III and forefinger pads.

FIGURE 11. Comparison between dummies and human soft tissues on the steady-state force. In (a)-(c), the steady-state forces of dummies were directly measured, while those of five human subjects were computed using Equation (6) and mean values of parameters γ_1. The light gray region denotes the steady-state force range. The abbreviation "Subj. 1–5" is for "human subject 1–5" in the legend.

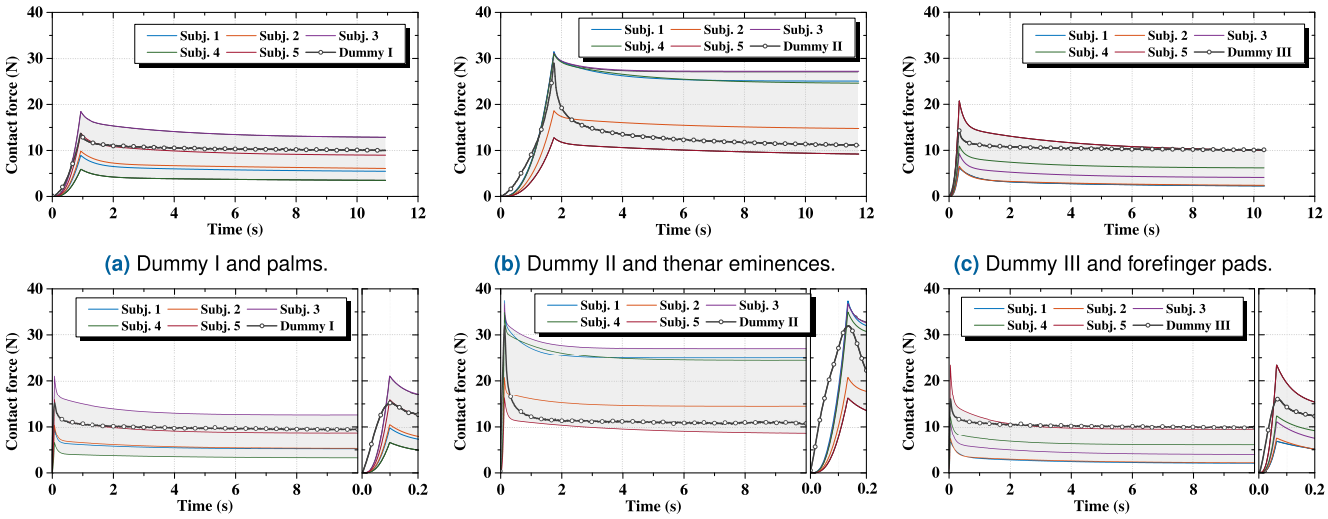

(a) Dummy I and palms. (b) Dummy II and thenar eminences. (c) Dummy III and forefinger pads.

(d) Dummy I and palms. (e) Dummy II and thenar eminences. (f) Dummy III and forefinger pads.

FIGURE 12. Comparison between dummies and human soft tissues on viscoelasticity. The contact condition of (a)=(c) is contact velocity of 10 mm/s and steady-state force of 10 N, while that of (d)-(f) is 250 mm/s and 10 N. In (a)-(f), contact force variations of the three dummies were obtained by measurement, while those of five human subjects were computed using the nonlinear viscoelastic model and mean values of parameters γ_1, γ_2, γ_3, c_2, and c_3. The light gray region denotes the force variation range. In (d)-(f), the graph on the right side shows the rising phase. The abbreviation "Subj. 1–5" is for "human subject 1–5" in the legend.

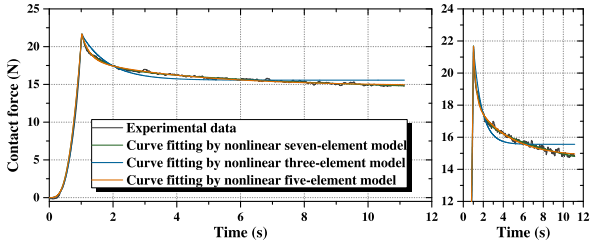

FIGURE 13. Comparison between the curve fitting result of the nonlinear three-, five-, and seven-element models. The graph on the right side shows details of the attenuation phase of the contact force.

in one layer in practice. According to the illustration of nonlinear springs and dampers, the proposed model can be expressed by a block diagram which allows simulations of the pHRI [35] to be easily realized. This is because, in the case of an arbitrary compressive displacement, the proposed model can be expressed as ordinary differential equations that make the establishment of a simulation easier and require less computing time, compared to that of the convolution form of the quasi-linear viscoelastic model.

In comparison to the previous study [31], the nonlinearity of stiffness is reasonably expressed by observing the fitting results of the attenuation phase; the proposed nonlinear model can be expressed by analytical formulas, which provide convenience for curve fitting. Moreover, as reported by Iki et al. [31], redundancy of the optimal solution existed in the curve fitting because of two elastic parameters associated with the steady-state force. There is no redundancy problem in this study because only γ_1 is related to the steady-state force, and the other four parameters are determined based on the principle stated at the beginning of this subsection.

Generally, the average of the viscoelastic parameters indicates the mechanical property of human soft tissue. However, the largest value of the viscoelastic parameters is considered as the optimal value for the dummy development owing to safety considerations. The dummies with larger

viscoelasticity contribute to a worse contact case wherein a larger contact force appears under the same contact situation, e.g., higher elasticity leads to a larger steady-state force, and higher viscosity suppresses the attenuation of contact force.

B. BIOFIDELITY OF THE DUMMIES

This study demonstrates two approaches for testing the biofidelity of dummies: a parametric comparison and calibration by ranges. The two approaches exhibited reliability for dummies I and II; however, the initial approach failed for dummy III. As indicated by the behavior of parameter γ_1 in Fig. 9(g), dummy III exhibited a larger steady-state elasticity than that of the forefinger pads, whereas a similar steady-state elasticity was observed in Fig. 11(c). This is because dummy III possesses a lower nonlinearity of elasticity than that of forefinger pads when the steady-state force is below 5 N, and parameter γ_1 is increased in the case where the lower nonlinearity part is used to conduct the curve fitting to optimize γ_1. Therefore, the parametric comparison is not suitable for examining the biofidelity of the developed dummies. Nevertheless, it demonstrates simplification and reliability when the dummy has the same nonlinearity of elasticity as the human soft tissue.

Considering the importance of the dynamic response of the contact force as stressed by [9], additional discussions on the calibration by ranges are presented. The calibration based on the ranges is more intuitive because it transforms parameter γ_1 to the calibration curves of the steady-state elasticity and parameters γ_1, γ_2, γ_3, c_2, and c_3 to those of the dynamic response of the contact force.

An elasticity range was accepted in the development of the Hybrid III dummy for the automobile industry [36], and the biofidelity of dummies is tested based on either the related injury criterion [14], [15] or the frequency domain [29]. This study employed a method that is similar to that describing the range of the elasticity regarding the test method in a previous study [36] and extended it to the ranges of elasticity and viscosity. The biofidelity was assessed depending on whether both the steady-state force and dynamic response of the contact force of the dummies are located within a steady-state force range and a force variation range, respectively. The two ranges were provided based on the individual differences of the human subjects, as shown in Figs. 11 and 12.

All three dummies, particularly dummies I and III, lost the biofidelity at the beginning of the contact. However, an elasticity exceeding that of the human soft tissue only appeared when the compressive displacement was small, and the steady-state force was under 5 N. Such a low biofidelity does not affect the performance in safety-validation experiments where a large contact force or compressive displacement results in the loss of safety. Moreover, a convexity was observed in the rising phase of the dummies when the contact velocity was 250 mm/s. the linear model may be also used for the case of high-velocity impact to represent the rising phase.

Dummies exhibit a nonlinearity of elasticity that differs from that of soft tissues. However, the high biofidelity of all three dummies is embodied in the large compressive displacement case, or when the steady-state force exceeds approximately 5 N.

Dummy I represents the average viscoelasticity of the five human subjects. This is observed from the fact that the steady-state force is located at the center of the steady-state force range, as well as the dynamic response of the contact force. In general, dummy I shows a more optimized standard for human palms.

Because dummy II shows a low steady-state force close to the lower edge of the steady-state force range, it may not be precise enough to monitor slight contact in the much smaller range of the pain onset level. However, its viscosity compensates for such low elasticity and enhances the rising phase of its contact force at the upper edge of the force variation range. Dummy II is expected to be used for studies involving the total energy injury criterion [11], [12] because such energy variation is calculated through an integral of the contact force from 0 to that corresponding to the maximum compressive displacement $x\left(t_p\right)$ in Equation (1), that is, the rising phase of the contact force.

Dummy III, with the largest steady-state elasticity, can help to build a safe–side dummy, coinciding with the safety consideration stressed in Section V-A. Dummy III is a suitable substitute for the forefinger pad in safety-validation experiments of the pHRI.

Moreover, dummy II has a higher nonlinear curvature than those of dummies I and III. This is attributed to the fact that the thickness plays a dominant role in the nonlinearity of the elasticity, and dummy II has the largest thickness (20 mm). This indicates that both the material characteristics and the thickness of the dummy changes the elasticity, which gives us more opportunities for developing dummies with the mechanical property of high similarity to that of the human soft tissue.

C. LIMITATION

The proposed experimental methodology cannot guarantee high repeatability of the impact between the impactor and soft tissue, because it would necessitate stricter fixation for the hand. However, a stricter fixation would increase hazards to the subjects and disregard ethical considerations.

Based on observations, it is inferred that the viscous parameters may have concealed relationships with the contact velocity. However, owing to the lack of contact velocity settings, the nonlinearity of viscous parameters was not considered in this study. The impedance properties can be acquired by modeling the contact force in a manner that is dependent only on inputs, that is, using the compressive displacement and contact velocity.

To the best of our knowledge, reports on the specific requirements of the elasticity for dummy development are rare. A specification, as well as characteristic similarity requirement for developing dummies, requires statistical results based on numerous experiments on human subjects. Because the number of human subjects, which was five in

the study, is small, it is difficult to propose a parametric specification. Nevertheless, this study emphasizes the development process of dummies, which is expected to promote quantifiable approaches to the development of dummies.

The biofidelity of the three dummies was embodied in the displacement–force calibration. The dummies were developed for the safety validation experiment of pHRI, and they are expected to be impacted in a pHRI environment instead of human soft tissues. The contact force/pressure are regarded as injury criteria to determine the safety level according to [9]. Therefore, the displacement–force similarity is sufficient for the dummies to mimic the performance of generating contact force/pressure. However, the thickness was not taken into account for the above safety validation, and the strain–stress similarity was not adopted in this study.

VI. CONCLUSION

This study devised a development process of high-biofidelity dummies as substitutes for human soft tissues used in hazardous pHRI experiments. A psychophysiological experiment was designed and conducted to obtain the dynamic response force of human hands under a worst-case clamping scenario. The center of the palm, thenar eminence, and forefinger pad were selected as the three specific soft tissues for the impact experiment. Then, a linear five-element Maxwell model was employed to fit the attenuation phase of the contact force variation. Consequently, a nonlinear five-element Maxwell model was proposed based on the observation of the nonlinearity of elastic parameters. The curve fitting results show unexpected performance in matching the rising phase of the contact force. Using the proposed nonlinear viscoelastic model, the viscoelasticity of the three soft tissues was quantified as five viscoelastic parameters.

Based on the viscoelasticity analysis of the three soft tissues, three dummies were fabricated using a polyurethane resin material. The biofidelity of the dummies was examined via parametric and curve comparisons. Based on the analysis of comparisons, the high biofidelity of all three dummies is embodied in the case where the steady-state force exceeds approximately 5 N. Dummy I represents the average elasticity and viscosity of the five human palms, and it shows a more optimized standard for fabricating the dummy for palms. Dummy III possesses the largest steady-state elasticity of forefinger pads to contribute to the fabrication of a safe–side dummy. However, dummy II shows a higher viscosity than that of the thenar eminences, thereby failing to fabricate either the standard dummy or the safe–side dummy.

Future studies will focus on improving the nonlinear viscoelastic model by revealing the nonlinearity of viscous parameters and enhancing the biofidelity of dummies by regulating the nonlinearity of their elasticity to reach a high similarity based on the strain–stress calibration. Moreover, considering that the shape of bone influences the viscoelasticity of the soft tissue, the structure of the human body parts will be considered for future dummy development.

ACKNOWLEDGMENT

The authors would like to thank TANAC Company Ltd., for their manufacturing technology support during the dummy development.

REFERENCES

[1] T. Ogure, Y. Nakabo, S. Jeong, and Y. Yamada, "Hazard analysis of an industrial upper-body humanoid," *Ind. Robot, Int. J.*, vol. 36, no. 5, pp. 469–476, Aug. 2009.
[2] B. Siciliano, O. Khatib, and T. Kröger, *Handbook of Robotics*, vol. 200. Berlin, Germany: Springer, 2008.
[3] P. Aivaliotis, S. Aivaliotis, C. Gkournelos, K. Kokkalis, G. Michalos, and S. Makris, "Power and force limiting on industrial robots for human-robot collaboration," *Robot. Comput.-Integr. Manuf.*, vol. 59, pp. 346–360, Oct. 2019.
[4] B. Yao, Z. Zhou, L. Wang, W. Xu, Q. Liu, and A. Liu, "Sensorless and adaptive admittance control of industrial robot in physical human-robot interaction," *Robot. Comput.-Integr. Manuf.*, vol. 51, pp. 158–168, Jun. 2018.
[5] E. Magrini, F. Flacco, and A. De Luca, "Control of generalized contact motion and force in physical human-robot interaction," in *Proc. IEEE Int. Conf. Robot. Autom. (ICRA)*, May 2015, pp. 2298–2304.
[6] A. De Luca, A. Albu-Schaffer, S. Haddadin, and G. Hirzinger, "Collision detection and safe reaction with the DLR-III lightweight manipulator arm," in *Proc. IEEE/RSJ Int. Conf. Intell. Robots Syst.*, Oct. 2006, pp. 1623–1630.
[7] S. Haddadin, A. Albu-Schäffer, and G. Hirzinger, "Requirements for safe robots: Measurements, analysis and new insights," *Int. J. Robot. Res.*, vol. 28, nos. 11–12, pp. 1507–1527, 2009.
[8] *Safety of Machinery—General Principles for Design—Risk Assessment and Risk Reduction*, Standard ISO 12100:2010, 2010.
[9] *Robots and Robotic Devices—Collaborative Robots*, Standard ISO/TS 15066:2016, 2016.
[10] S. Haddadin, S. Haddadin, A. Khoury, T. Rokahr, S. Parusel, R. Burgkart, A. Bicchi, and A. Albu-Schäffer, "On making robots understand safety: Embedding injury knowledge into control," *Int. J. Robot. Res.*, vol. 31, no. 13, pp. 1578–1602, 2012.
[11] T. Fujikawa, R. Sugiura, R. Nishikata, and T. Nishimoto, "Critical contact pressure and transferred energy for soft tissue injury by blunt impact in human-robot interaction," in *Proc. 17th Int. Conf. Control, Autom. Syst. (ICCAS)*, Oct. 2017, pp. 867–872.
[12] R. Sugiura, T. Fujikawa, R. Nishikata, and T. Nishimoto, "Soft tissue bruise injury by blunt impact in human-robot Interaction–Difference of tolerance between chest and extremities," in *Proc. 19th Int. Conf. Control, Autom. Syst. (ICCAS)*, Oct. 2019, pp. 792–797.
[13] S. Oberer and R. D. Schraft, "Robot-dummy crash tests for robot safety assessment," in *Proc. IEEE Int. Conf. Robot. Autom.*, Apr. 2007, pp. 2934–2939.
[14] S. Haddadin, A. Albu-Schäffer, and G. Hirzinger, "Safety evaluation of physical human-robot interaction via crash-testing," in *Robotics: Science and systems*, vol. 3. MIT Press, 2007, pp. 217–224.
[15] S. Haddadin, A. Albu-Schäffer, and G. Hirzinger, "Approaching Asimov's 1st law: The impact of the robot's weight class," in *Robotics: Science and Systems*. Atlanta, GA, USA: Citeseer, 2007.
[16] B. F. Herbst, "Fidelity of anthropometric test dummy necks in rollover accidents," in *Proc. Int. Tech. Conf. Enhanced Saf. Vehicles*, vol. 1998, 1998, pp. 2093–2097.
[17] P. Tanyaporn, S. Yusaku, O. Tamao, and W. Ryoji, "Contact area effects on superficial and deep pain threshold for service robot safety design using a pain-sensing system: Development of a human-inspired pain-sensing system," *Panasonic Tech. J.*, vol. 65, no. 1, pp. 21–26, 2019.
[18] F. Li, Y. Akiyama, X. Wan, S. Okamoto, and Y. Yamada, "Measurement of shear strain field in a soft material using a sensor system consisting of distributed piezoelectric polymer film," *Sensors*, vol. 20, no. 12, p. 3484, Jun. 2020.
[19] Y. Fung, *Biomechanics: Mechanical Properties of Living Tissues*. New York, NY, USA: Springer, 2013.
[20] U. Dombrowski, T. Stefanak, and A. Reimer, "Simulation of human-robot collaboration by means of power and force limiting," *Proc. Manuf.*, vol. 17, pp. 134–141, Jan. 2018.
[21] H. Delingette, "Toward realistic soft-tissue modeling in medical simulation," *Proc. IEEE*, vol. 86, no. 3, pp. 512–523, Mar. 1998.

[22] J. Kim and M. A. Srinivasan, "Characterization of viscoelastic soft tissue properties from in vivo animal experiments and inverse fe parameter estimation," in *Proc. Int. Conf. Med. Image Comput.-Assist. Intervent.* Berlin, Germany: Springer, 2005, pp. 599–606.
[23] M. Bro-Nielsen, "Modelling elasticity in solids using active cubes-application to simulated operations," in *Proc. Int. Conf. Comput. Vis., Virtual Reality, Robot. Med.* Berlin, Germany: Springer, 1995, pp. 535–541.
[24] C. E. Jamison, R. D. Marangoni, and A. A. Glaser, "Viscoelastic properties of soft tissue by discrete model characterization," *J. Biomech.*, vol. 1, no. 1, pp. 33–46, Jan. 1968.
[25] W. F. Larrabee, "A finite element model of skin deformation. i. biomechanics of skin and soft tissue: A review," *Laryngoscope*, vol. 96, no. 4, pp. 399–405, 1986.
[26] C. Escoffier, J. de Rigal, A. Rochefort, R. Vasselet, J.-L. Lévêque, and P. G. Agache, "Age-related mechanical properties of human skin: An in vivo study," *J. Investigative Dermatology*, vol. 93, no. 3, pp. 353–357, Sep. 1989.
[27] A. Nava, E. Mazza, F. Kleinermann, N. J. Avis, and J. McClure, "Determination of the mechanical properties of soft human tissues through aspiration experiments," in *Proc. Int. Conf. Med. Image Comput.-Assist. Intervent.* Berlin, Germany: Springer, 2003, pp. 222–229.
[28] N. Hogan, "Impedance control: An approach to manipulation," in *Proc. Amer. Control Conf.*, San Diego, CA, USA, Jun. 1984, pp. 304–313.
[29] M. Aso, Y. Yamada, K. Yoshida, Y. Akiyama, and Y. Ito, "Evaluation of the mechanical characteristics of human thighs for developing complex dummy tissues," in *Proc. IEEE Int. Conf. Robot. Biomimetics (ROBIO)*, Dec. 2013, pp. 1450–1455.
[30] N. Nakazawa, R. Ikeura, and H. Inooka, "Characteristics of human fingertips in the shearing direction," *Biol. Cybern.*, vol. 82, no. 3, pp. 207–214, Feb. 2000.
[31] Y. Iki, Y. Yamada, Y. Akiyama, S. Okamoto, and J. Liu, "Designing a dummy skin by evaluating contacts between a human hand and a robot end tip," in *Proc. IEEE/RSJ Int. Conf. Intell. Robots Syst. (IROS)*, Oct. 2020, pp. 11337–11344.
[32] J. Liu, Y. Yamada, and Y. Akiyama, "Calculating the supplied energy for physical human-robot interaction," in *Proc. IEEE Int. Conf. Intell. Saf. Robot. (ISR)*, Mar. 2021, pp. 157–160.
[33] *Robots and Robotic Devices—Safety Requirements for Industrial Robots—Part I: Robots*, Standard ISO 10218–1:2011, 2011.
[34] T. H. Shellhammer, T. R. Rumsey, and J. M. Krochta, "Viscoelastic properties of edible lipids," *J. Food Eng.*, vol. 33, nos. 3–4, pp. 305–320, 1997.
[35] J. Liu, Y. Yamada, Y. Akiyama, S. Okamoto, and Y. Iki, "A novel safety-oriented control strategy for manipulators based on the observation and adjustment of the external momentum," in *Proc. Int. Conf. Comput., Control Robot. (ICCCR)*, Jan. 2021, pp. 80–86.
[36] *Electronic Code of Federal Regulations (e-CFR), Title 49, Part 572.9*, U.S. Nat. Arch. Records Admin., 1973

JIAN LIU received the M.S. degree in mechanical and electronic engineering from Zhejiang University, Hangzhou, China, in 2018. He is currently pursuing the Ph.D. degree in mechanical systems engineering with Nagoya University, Nagoya, Japan. His current research interests include robotics, biomechanics, and especially physical human safety in human–robot coexistence systems.

YOJI YAMADA (Member, IEEE) received the Ph.D. degree from the Tokyo Institute of Technology. Since 1983, he has been with the Toyota Technological Institute, Nagoya, Japan. In 2004, he joined as a Leader with the Safety Intelligence Research Group, National Institute of Advanced Industrial and Science Technology (AIST). In 2009, he joined as a Professor with the Department of Mechanical Science and Engineering, Graduate School of Engineering, Nagoya University. In 2022, he joined as the President of the Toyota College, National Institute of Technology.

YASUHIRO AKIYAMA (Member, IEEE) received the B.E. degree in engineering from the Tokyo Institute of Technology, Tokyo, Japan, in 2006, and the M.S. and Ph.D. degrees in engineering from The University of Tokyo, Tokyo, in 2008 and 2011, respectively. From 2016 to 2022, he was an Assistant Professor with Nagoya University, Japan. He is currently an Associate Professor with Shinshu University. His main research interests include mechanical safety, human–robot interaction, and biomechanics.

SHOGO OKAMOTO (Member, IEEE) received the Ph.D. degree in information sciences from Tohoku University, in 2010. From 2010 to 2021, he was an Associate Professor with Nagoya University. He is currently an Associate Professor with the Department of Computer Science, Tokyo Metropolitan University. His research interests include haptics, assistive robotics, human-centered informatics, and affective engineering.

YUMENA IKI received the B.S. and M.S. degrees from Nagoya University, Nagoya, Japan, in 2019 and 2021, respectively.